
DiffGCN: Graph Convolutional Networks via Differential Operators and Algebraic Multigrid Pooling

Moshe Eliasof

Department of Computer Science
Ben-Gurion University of the Negev

Eran Treister

Department of Computer Science
Ben-Gurion University of the Negev

Abstract

Graph Convolutional Networks (GCNs) have shown to be effective in handling unordered data like point cloud and meshes. In this work we propose novel approaches for graph convolution, pooling and unpooling, taking inspiration from finite-elements and algebraic multigrid frameworks. We form a parameterized convolution kernel based on discretized differential operators, leveraging the graph mass, gradient and Laplacian. This way, the parameterization does not depend on the graph structure, only on the meaning of the network convolutions as differential operators. To allow hierarchical representations of the input, we propose pooling and unpooling operations that are based on algebraic multigrid methods. To motivate and explain our method, we compare it to standard Convolutional Neural Networks, and show their similarities and relations in the case of a regular grid. Our proposed method is demonstrated in various experiments like classification and segmentation, achieving on par or better than state of the art results. We also analyze the computational cost of our method compared to other GCNs.

1 Introduction

The emergence of deep learning and Convolutional Neural Networks (CNNs) [29, 23, 52] in recent years has had great impact on the community of computer vision and graphics [44, 9, 21, 24]. Over the past years, multiple works used standard CNNs to perform 3D related tasks over unordered data (e.g., point clouds and meshes), one of which is PointNet [39, 41], that operates directly on point clouds. Along with these works, another massively growing field is Graph Convolutional Networks (GCNs) or as we regard to it in this work – Geometric Deep Learning, which suggests using graph convolutions, arising from either spectral theory [5, 27, 11] or spatial representation [51, 35, 19, 37]. This makes the processing of unstructured data like point clouds, graphs and meshes more natural by operating directly in the underlying structure of the data.

In this work we aim to bridge the gap between ordered and unordered deep learning architectures, and build on the foundation of standard CNNs in unordered data. To this end, we leverage the similarity between standard CNNs and partial differential equations (PDEs) [47], and propose a new approach to define convolution operators on graphs that is based on discretization of differential operators on unstructured grids. Specifically, we define a 3D convolution kernel which is based on discretized differential operators. We consider the mass (self-feature), gradient and Laplacian of the graph and discretize them using a simple version of finite differences, similarly to the way that standard graph Laplacians are defined. Such differential operators form a subspace which spans standard convolution kernels on structured grids. Leveraging on such operators for unstructured grids leads to an abstract parameterization of the convolution operation, which is independent of the specific graph geometry.

Our second contribution involves the unstructured pooling and unpooling operators, which together with the convolution, are among the main building blocks of CNNs. To this end, and further motivated by the PDE interpretation of CNNs, we utilize multigrid methods which are among the most efficient numerical solvers for PDEs. Such methods use a hierarchy of smaller and smaller grids to represent the PDE on various scales. Specifically, algebraic multigrid (AMG) approaches [45, 32] are mostly used to solve PDEs on unstructured grids by forming the same hierarchy of problems using coarsening and upsampling operators. Using these building blocks of AMG, we propose novel pooling and unpooling operations for GCNs. Our operators are based on the Galerkin coarsening operator of aggregation-based AMG [54], performing pure aggregation for pooling and smoothed aggregation as the unpooling operator. The advantage of having pooling capability, as seen both in traditional CNNs and GCNs [44, 22, 9, 21] are the enlargement of the receptive field of the neurons, and reduced computational cost (FLOP-wise), allowing for wider and deeper networks.

In what follows, we elaborate on existing unordered data methods in section 2, and present our method in section 3. We discuss the similarity between traditional CNNs and our proposed GCN, and the purpose of using differential operators as a parameterization to a convolution kernel in Section 3.3, and compare the computational costs of our method compared to other message-passing, spatially based GCNs in Section 3.5. To validate our model, we perform experiments on point cloud classification and segmentation tasks on various datasets in section 4. Finally, we study the importance and contribution of the different terms in the parameterization to the performance of our method in Section 5, as well as report quantitative results of our network with different differential-operator terms, i.e., using various combinations of them.

2 Related work

Unordered data come in many forms and underlying structures – from meshes and point clouds that describe 3D objects to social network graphs. For 3D related data, a natural choice would be to voxelize the support of the data, as in [36]. Clearly, such approach comes at a high computational cost, while causing degradation of the data. Other methods suggest to operate directly on the data - whether it is a point cloud [39, 41, 30] or a graph [11, 35, 5, 27, 56].

Recent works like [35, 37] assumed a system of local coordinates centered around each vertex. These methods propose to assign weights to geometric neighborhoods around the vertices, in addition to the filter weights. Masci et al. [35] proposed assigning fixed Gaussian mixture weight for those neighborhoods, and [37] goes a step further and learns the parameters of the Gaussians. These methods require high computational costs, due to the computation of exponential terms (particularly at inference time) as well as the overhead of additional learnable parameters.

Later, it was shown in [56] that adapting GCNs for point-cloud related tasks can be highly beneficial, since the learned features of the graph vertices in different layers of the network induce graphs which reveal their underlying correlations. We follow the trend of employing GCNs for point-cloud related tasks like shape classification and segmentation. Specifically, we choose to work with spatial GCNs since they are not dependent on eigen-vectors of a specific graph, unlike spectral GCNs. However, compared to other works like DGCNN[55] and MPNN [19] which in some sense also use discretized gradient operators, we introduce the addition of the Laplacian term of the graph. This is a major building block in spectral-based methods like [11, 27], but was not used in spatial GCNs where the vertices have a geometric meaning, to the best of our knowledge.

Unlike traditional structured CNNs, where the pooling and unpooling operations are trivial, these operations are more debatable in unordered methods, due to the lack of order or the metric between points. Works like PointNet++ [41] proposed using Furthest Point Sampling technique in order to choose remaining points in coarsened versions of the inputs. Others [21, 18] proposed utilizing ℓ_2 norm of the features to determine which elements of the graph are to be removed in subsequent layers of the network. Additional works like DiffPool[60] proposed learning a dense assignment matrix to produce coarsened version of an initial graph. However, learning a dense matrix is of quadratic computational cost in the number of vertices and does not scale well for large scale point-clouds.

We focus on the employment of AMG as a concept to define our pooling/unpooling operation. We use classical AMG, which is suitable for unstructured grids, similarly to works that incorporated geometric multigrid concepts into structured grids CNNs [9, 25]. On a different note, the recent work [34] showed another connection between AMG and GCNs, and proposed using GCNs for

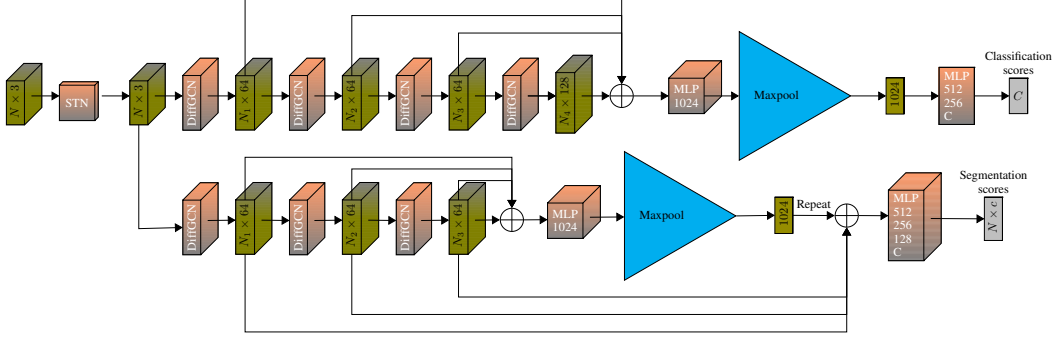


Figure 1: Our architectures for classification (upper part) and segmentation (lower part) tasks. STN denotes a spatial transformer module [39]. Channel-wise concatenation is denoted by \oplus . N_i denotes the number of vertices after the i -th DiffGCN block.

learning sparse AMG prolongation matrices to solve weighted diffusion problems on unstructured grids.

3 Method

We propose to parameterize the graph convolutional kernel according to discretized differential operators defined on a graph. Therefore, we call our convolution DiffGCN. To have a complete set of neural network building blocks, we also propose an AMG inspired pooling and unpooling operators to enlarge the receptive fields of the neurons, and to allow for wider and deeper networks.

3.1 Convolution kernels via differential operators

To define the convolution kernels in the simplest way, we use finite differences, which is a simple and a widely used approach for numerical discretization of differential operators. Alternatives, such as finite element or finite volume schemes may also be suitable for the task, but are more complicated to implement in existing deep learning frameworks. Using finite differences, the first and second order derivatives are approximated as:

$$\frac{\partial f(x)}{\partial x} \approx \frac{f(x+h) - f(x-h)}{2h}, \quad \frac{\partial^2 f(x)}{\partial x^2} \approx \frac{f(x+h) - 2f(x) + f(x-h)}{h^2}. \quad (1)$$

We harness these simple operators to estimate the gradient and Laplacian of the unstructured feature maps defined on a graph.

Given an undirected graph $\mathcal{G} = (V, E)$ where V, E denote the vertices and edges of the graph, respectively, we propose a formulation of the convolution kernel as follows:

$$\text{conv}(\mathcal{G}, \Theta) = \theta_1 I + \theta_2 \frac{\partial}{\partial x} + \theta_3 \frac{\partial^2}{\partial x^2} + \theta_4 \frac{\partial}{\partial y} + \theta_5 \frac{\partial^2}{\partial y^2} + \theta_6 \frac{\partial}{\partial z} + \theta_7 \frac{\partial^2}{\partial z^2}. \quad (2)$$

This gives a 7 point-based stencil convolution operator which makes use of the mass, gradient and Laplacian of the signal defined over the graph.

We now formulate the operators in (2) mathematically. We first define that the features of the GCN are located in vertices $v_i \in V$ of the graph (similarly to a nodal discretization). We start with the definition of the gradient (in x, y, z), which according to (1) is defined on the middle of an edge $e_{ij} \in E$ connecting the pair v_i and v_j . Since the edge direction may not be aligned with a specific axis, we project the derivative along the edge onto the axes x, y, z . For example,

$$\frac{\partial f}{\partial x}(e_{ij}) = \frac{f_{v_i} - f_{v_j}}{2\text{dist}(v_i, v_j)}(x_{v_i} - x_{v_j}). \quad (3)$$

$x(v_i)$ is the x -location of vertex v_i , and $f(v_i)$ is the feature vector defined on vertex v_i . $\text{dist}(v_i, v_j)$ is the Euclidean distance between v_i and v_j . Given this approach, we define the gradient matrix of

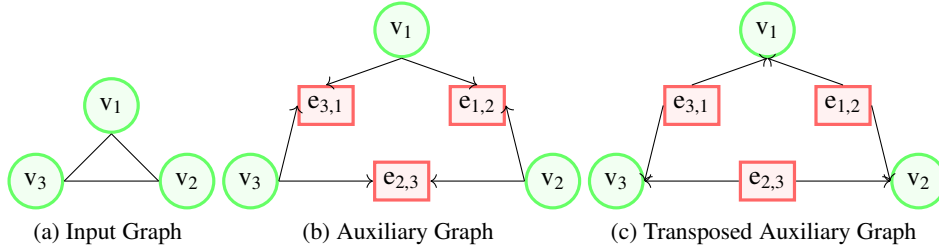


Figure 2: Example of a graph and its Auxiliary and transposed Auxiliary graphs which are used to implement our method as described in section 3.1.

the graph by stacking the projected differential operator in each of the directions

$$\nabla_{\mathcal{G}} = \begin{bmatrix} \partial_{\mathcal{G}}^x \\ \partial_{\mathcal{G}}^y \\ \partial_{\mathcal{G}}^z \end{bmatrix} : |V| \rightarrow 3 \cdot |E| \quad (4)$$

This gradient operates on vertex space and its output size is 3 times the edge space for the x, y, z directions. To gather the gradients back to the vertex space we form an edge-averaging operator

$$A : 3 \cdot |E| \rightarrow 3 \cdot |V|, \quad (Af)_i = \frac{1}{|\mathcal{N}_e(v_i)|} \sum_{j \in \mathcal{N}_e(v_i)} f_{ij} \quad (5)$$

where $\mathcal{N}_e(v_i) = \{j : e_{ij} \in E\}$ is the set of edges associated with vertex v_i . The function f in (5) is a feature map tensor defined on the edge space of the graph.

In a similar fashion, the Laplacian of the graph w.r.t each axis (x, y, z) is computed in two steps. The first step is the same as in equation (4). Then, we apply the following transposed first derivative operators (similarly to a discretized divergence, only we do not sum the derivatives) to obtain the second derivatives back on the vertices:

$$\begin{bmatrix} (\partial_{\mathcal{G}}^x)^T & 0 & 0 \\ 0 & (\partial_{\mathcal{G}}^y)^T & 0 \\ 0 & 0 & (\partial_{\mathcal{G}}^z)^T \end{bmatrix} : 3 \cdot |E| \rightarrow 3 \cdot |V|. \quad (6)$$

This construction is similar to the way graph Laplacians and finite element Laplacians are defined on graphs or unstructured grids.

Implementation using PyTorch-Geometric To obtain such functionality while using common GCN-designated software [17] and concepts [51, 19], we define a directed *auxiliary* graph denoted by $\mathcal{G}' = (V', E')$, where in addition to the original set of vertices V , we have the mid-edge locations $e_{ij} \in E$. Then, we define the connectivity of \mathcal{G}' such that each vertex $v_i \in V$ has a direct connection to the mid-edge location e_{ij} as in Fig. 2. More explicitly:

$$V' = V \cup E, \quad E' = \{(v_i, e_{ij}), (v_j, e_{ij}) \mid e_{ij} \in E\}. \quad (7)$$

We also use the transposed graph, which is an edge flipped version of \mathcal{G}' , also demonstrated in Fig. 2.

Given these two graphs, we are able to obtain the gradient and Laplacian terms of the signal defined over the graph via mean aggregation of message passing scheme [19, 51], where we perform two stages of the latter. First, we use the auxiliary graph \mathcal{G}' to send the following message:

$$message_{Grad}(v_i, e_{ij}) = \frac{f_{v_i}}{2dist(v_i, e_{ij})} \left(\begin{bmatrix} x(v_i) \\ y(v_i) \\ z(v_i) \end{bmatrix} - \begin{bmatrix} x(e_{ij}) \\ y(e_{ij}) \\ z(e_{ij}) \end{bmatrix} \right) \in \mathbb{R}^{3|f_{v_i}|}, \quad (v_i, e_{ij}) \in E' \quad (8)$$

Here, each vertex gets two messages, and due to the subtraction in the message, the discretized gradient is obtained on the edges. Following this, we return a double message over the transposed

\mathcal{G}' , returning both the gradient and the Laplacian of the graph on the original vertex space. The first part of the message averages the gradient terms from the edges to the vertices

$$message_{EdgeAvg}(e_{ij}, v_i) = f_{e_{ij}}, \quad (v_i, e_{ij}) \in E'. \quad (9)$$

The second part of the message differentiates the edge gradients to obtain the Laplacian:

$$message_{Lap}(e_{ij}, v_i) = \frac{f_{e_{ij}}}{2dist(v_i, e_{ij})} \left(\begin{bmatrix} x(e_{ij}) \\ y(e_{ij}) \\ z(e_{ij}) \end{bmatrix} - \begin{bmatrix} x(v_i) \\ y(v_i) \\ z(v_i) \end{bmatrix} \right) \in \mathbb{R}^{3 \cdot |f_i|}, \quad (v_i, e_{ij}) \in E'. \quad (10)$$

Then, we perform mean aggregation of these messages and concatenate them:

$$\hat{f}_i = f_i \oplus Grad_{\mathcal{G}}(v_i) \oplus Lap_{\mathcal{G}}(v_i) \in \mathbb{R}^{7 \cdot |V|}, \quad (11)$$

where \oplus denotes channel-wise concatenation. Finally, we apply a multi-layer perceptron (MLP)—a $c_{out} \times 7 \cdot c_{in}$ point-wise convolution followed by batch normalization and ReLU—to the features in Eq. (11).

3.2 Algebraic multigrid pooling and unpooling

An effective pooling operation is highly important to faithfully represent coarsened versions of the graph. We propose to use AMG methods [54, 32], namely, the Galerkin coarsening which we explain now.

In AMG methods the coarse graph vertices are typically chosen as either a subset of the fine graph vertices (dubbed ‘‘C-points’’) or as clusters of vertices called aggregates. We use the latter approach, and apply the Graclus clustering [12] to form the aggregates. Let $\{\mathcal{C}_J\}_{J=1}^{V_{coarse}}$ be the aggregates, each correspond to a vertex in the coarse graph. Then, we define the restriction (pooling) operator:

$$R_{J,i} = \begin{cases} 1 & i \in \mathcal{C}_J \\ 0 & otherwise \end{cases}. \quad (12)$$

The features and adjacency matrix of the coarsened graph are defined using Galerkin coarsening:

$$X^{coarse} = R^T X, \quad A^{coarse} = R^T A R \in \mathbb{R}^{|V| \times |V|}. \quad (13)$$

To perform the unpooling operator, also called prolongation, we may use the transpose of the restriction operator (12). However, when unpooling with an aggregation matrix, we get piece-wise constant feature maps, which are undesired. To have a smoother unpooling operator, we propose to allow the prolongation of soft clustering via *smoothed* aggregation [54] as follows:

$$P = (I - (D)^{-1}L)R^T \in \mathbb{R}^{|V| \times |V_{coarse}|} \quad (14)$$

Where I, D, L is the identity matrix, degree and Laplacian matrix of the layer, respectively. To unpool from a coarsened version of the graph, we apply the corresponding prolongation operator at each level, until we reach the initial problem resolution.

3.3 Similarity between DiffGCN and standard CNN operators for structured grids

A standard CNN is based on learning weights of convolutional filters. The work [47] showed that the 2D convolution kernel can be represented as a linear combination of finite difference differential operators. These classical differential operators are obtained using our definitions in Eq. (3)-(6), in the case of a structured regular graph. In 2D (without the z axis), Eq. (2) will result in a 5-point stencil represented as

$$\theta_1 \begin{bmatrix} 0 & 0 & 0 \\ 0 & 1 & 0 \\ 0 & 0 & 0 \end{bmatrix} + \theta_2 \begin{bmatrix} 0 & 0 & 0 \\ -1 & 0 & 1 \\ 0 & 0 & 0 \end{bmatrix} + \theta_3 \begin{bmatrix} 0 & 0 & 0 \\ 1 & -2 & 1 \\ 0 & 0 & 0 \end{bmatrix} + \theta_4 \begin{bmatrix} 0 & 1 & 0 \\ 0 & 0 & 0 \\ 0 & -1 & 0 \end{bmatrix} + \theta_5 \begin{bmatrix} 0 & 1 & 0 \\ 0 & -2 & 0 \\ 0 & 1 & 0 \end{bmatrix} \quad (15)$$

The Laplacian, together with the mass term allow the network to obtain low-pass filters, that are highly important to average out noise, and to prevent aliasing when downsampling the feature-maps. Gradient based methods like [56] can only approximate the Laplacian term via multiple convolutions,

leading to redundant computations. Furthermore, the work of [14] showed that the popular 3×3 convolution kernel can be replaced by this 5 point stencil without losing much accuracy. When extending this to 3D, the common $3 \times 3 \times 3$ kernel includes 27 weights, and the leaner version in (2) ends in a star-shaped stencil using 7 weights only, which is a significant reduction from 27. We refer the interested reader to [20, 7, 57, 8, 33, 10] for a more rigorous study of the connection between ODEs, PDEs and CNNs.

3.4 DiffGCN architectures

We show the architectures used in this work in Fig. 1. We define a DiffGCN block which consists of two DiffGCN convolutions, with a shortcut connection, as in ResNet [22] for better convergence and stability. Pooling is performed before the first convolution in each block, besides the first opening layer. We use concatenating skip-connections to fuse feature maps from shallow and deep layers. Before this concatenation, unpooling is performed to resize the point-cloud to its original dimensions.

3.5 Computational cost of DiffGCN

Typically, spatial GCNs like [51, 19, 56, 35] employ the convolutions K times per vertex, where K is the neighborhood size. More explicitly, a typical convolution can be written as

$$x'_i = \square_{j \in \mathcal{N}(i)} h_{\Theta}(f(x_i, x_j)), \quad (16)$$

where $\mathcal{N}(i)$ is the set of neighbors of vertex $i \in V$, \square is a permutation invariant aggregation operator like max or sum and h_{Θ} is an MLP [39] parameterized by the set of weights Θ . f is a function that is dependent on a vertex and its neighbors. For instance, in DGCNN [56] $f(x_i, x_j) = x_i \oplus (x_i - x_j)$. By design, our convolution operation first gathers the required differential terms, and then feeds their channel-wise concatenation through a MLP. That is our convolution can be written as

$$x'_i = h_{\Theta}(\square_{j \in \mathcal{N}(i)} g(x_i, x_j)), \quad (17)$$

where g is a function that constructs the desired differential operator terms. Thus, we reduce the feed-forward pass of our convolution by an order of K , which decreases the number of FLOPs required in our convolution. In other words, the MLP operation in our convolution is independent of the number of neighbors K , since we aggregate the neighborhood features prior to the MLP. If N is the input size, and c_{in} , c_{out} are the number of input and output channels, respectively, then the number of floating point operations of a method defined via Eq. (16) is $N \times K \times c_{in} \times c_{out}$, while the cost of our method reduces to $N \times c_{in} \times c_{out}$. In Table 1 we report the amount of FLOPs for various convolutions with 1,024 points input and $c_{in} = 64$, $c_{out} = 128$. For VoxNet [36] we use a $3 \times 3 \times 3$ kernel, and for PointCNN, DGCNN and ours, we set the neighborhood size $K = 10$.

Table 1: A comparison of single convolution FLOPs.

VoxNet [36]	PoinetNet (MLP) [39]	PointCNN [30]	DGCNN [56]	DiffGCN (ours)
7247.75M	8.39M	122.62M	167.78M	61.3M

4 Experiments

To demonstrate the effectiveness of our framework, we conducted three experiments on three different datasets - classification (ModelNet40 [58]), part segmentation (ShapeNet Parts [59]) and semantic segmentation (S3DIS [1]). We also report an ablation study to obtain a deeper understanding of our framework. In all the experiments, we start from a point-cloud, and at each DiffGCN block we construct a K-nearest-neighbor graph according to the features of the points.

We implement our work using the PyTorch [38] and PyTorch Geometric [17] libraries. We use the networks shown in Fig. 1. For the semantic segmentation task on S3DIS we do not use a spatial transformer. Throughout all the experiments we use ADAM optimizer [26] with initial learning rate of 0.001. We run our experiments using NVIDIA Titan RTX with batch size 20. Our loss function is the cross-entropy loss for classification and focal-loss [31] for the segmentation tasks.

Table 2: Classification results on ModelNet40. Metric is in pixel accuracy.

Method	Mean Class Accuracy	Overall Accuracy
3DShapeNets [58]	77.3	84.7
VoxNet [36]	83.0	85.9
Subvolume [40]	86.0	89.2
VRN (single view) [3]	88.98	—
VRN (multiple views) [3]	91.33	—
ECC [51]	82.3	87.4
PointNet [39]	86.0	89.2
PointNet++ [41]	—	90.7
Kd-net [28]	—	90.7
PCNN [2]	—	92.3
PointCNN [30]	88.1	92.2
KCNet [50]	—	91.0
DGCNN [56] (K=20)	90.2	92.9
DGCNN [56] (K=10)	88.9	91.4
LDGCNN [61]	90.3	92.9
Ours (K=20)	90.4	93.5
Ours (K=20, pooling)	90.7	93.9

Table 3: ShapeNet part segmentation. Results shown in mean intersection over union metric.

	Aero	Bag	Cap	Car	Chair	Earphone	Guitar	Knife	Lamp	Laptop	Motor	Mug	Pistol	Rocket	Skateboard	Table	Mean
Shapes	2690	76	55	898	3578	69	787	392	1547	451	202	184	283	66	152	5271	
PointNet [39]	83.4	78.7	82.5	74.9	89.6	73.0	91.5	85.9	80.8	95.3	65.2	93.0	81.2	57.9	72.8	80.6	83.7
PointNet++ [41]	82.4	79.0	87.7	77.3	90.8	71.8	91.0	85.9	83.7	95.3	71.6	94.1	81.3	58.7	76.4	82.6	85.1
KD-Net [28]	80.1	74.6	74.3	70.3	88.6	73.5	90.2	87.2	81.0	94.9	57.4	86.7	78.1	51.8	69.9	80.3	82.3
LocalFeatureNet [49]	86.1	73.0	54.9	77.4	88.8	55.0	90.6	86.5	75.2	96.1	57.3	91.7	83.1	53.9	72.5	83.8	84.3
PCNN [2]	82.4	80.1	85.5	79.5	90.8	73.2	91.3	86.0	85.0	95.7	73.2	94.8	83.3	51.0	75.0	81.8	85.1
PointCNN [30]	84.1	86.45	86.0	80.8	90.6	79.7	92.3	88.4	85.3	96.1	77.2	95.3	84.2	64.2	80.0	83.0	86.1
KCNet [50]	82.8	81.5	86.4	77.6	90.3	76.8	91.0	87.2	84.5	95.5	69.2	94.4	81.6	60.1	75.2	81.3	84.7
DGCNN [56]	84.0	83.4	86.7	77.8	90.6	74.7	91.2	87.5	82.8	95.7	66.3	94.9	81.1	63.5	74.5	82.6	85.2
LDGCNN [61]	84.0	83.0	84.9	78.4	90.6	74.4	91.0	88.1	83.4	95.8	67.4	94.9	82.3	59.2	76.0	81.9	85.1
Ours	85.1	83.1	87.2	80.9	90.9	79.8	92.1	87.8	85.2	96.3	76.6	95.8	84.2	61.1	77.5	83.6	86.4
Ours (pooling)	85.1	83.7	88.0	80.3	91.1	80.0	92.0	87.5	85.3	95.8	76.0	95.9	83.8	65.6	77.3	83.7	86.4

4.1 Classification results

For the classification task we use ModelNet-40 dataset [58] which includes 12,311 CAD meshes across 40 different categories. The data split is as follows: 9,843 for training and 2,468 for testing. Our training scheme is similar to the one proposed in PointNet [39], in which we rescale each mesh to a unit cube, and then we sample 1,024 random points from each mesh at each epoch. We also use random scaling between 0.8 to 1.2 and add random rotations to the generated point cloud. We report our results with $K = 20$, with and without pooling. The results of our method are summarized in Table 2. We obtained higher accuracy than [56, 50, 61] which also use GCNs for this task. We suggest that the difference stems mainly from the addition of the Laplacian term to our convolution, and the contribution of the pooling module. Note, the work HGNN [15] which is based on hypergraphs, using features that are of size 4,096 (and not only 3), extracted from MVCNN [53] and GVCNN [16], therefore, we do not include it in Table 2.

4.2 Segmentation results

We test our method on two different segmentation datasets - Shapenet part segmentation [59] and Stanford Large-Scale 3D Indoor Spaces Dataset (S3DIS) [1]. We use the lower part network in Fig. 1, with $K = 20, 10, 5$ in each of the DiffGCN blocks, respectively. For Shapenet part segmentation dataset, our objective is to classify each point in a point-cloud to its correct part category. There are 16,881 3D shapes across 16 different categories, with a total of 50 part annotation classes, where each shape is annotated with 2-6 parts. We sample 2,048 points from each shape and use the training, validation and testing split in [6]. The results are reported in Table 3. Our method achieves the highest mIoU out of all the considered networks.

Table 4: Semantic segmentation results on Stanford Large-Scale 3D Indoor Spaces Dataset (S3DIS). Results shown in mean intersection over union metric.

Method	mIoU	Overall Accuracy
PointNet (baseline) [39]	20.1	53.2
PointNet [39]	47.6	78.5
MS + CU(2) [13]	47.8	79.2
G + RCU [13]	49.7	81.1
PointCNN [30]	65.4	—
DGCNN [56]	56.1	84.1
DCM-Net [48]	64.0	—
Ours	57.2	84.9
Ours (pooling)	56.9	84.5

Table 5: Ablation study results on ModelNet40. Metric is in pixel accuracy.

Variation	Mean Class Accuracy	Overall Accuracy
Mass+Grad+Lap (K=10)	89.1	92.7
Mass+Grad+Lap (K=10, w.pooling)	89.5	93.1
Mass+Grad+Lap (K=5)	88.7	92.1
Mass+Grad+Lap (K=5, w.pooling)	88.9	92.3
Mass Only (K=20)	85.4	88.2
Grad Only (K=20)	79.9	85.0
Lap Only (K=20)	79.2	83.2
Mass + Grad (K=20)	88.3	91.0
Mass + Lap (K=20)	88.6	91.9

The Stanford Large-Scale 3D Indoor Spaces Dataset (S3DIS) contains 3D scans of 272 room from 6 different areas. Each point is annotated with one of 13 semantic classes. We adopt the pre-processing steps of splitting each room into $1m \times 1m$ blocks with random 4,096 points at the training phase, and all points during, where each point represented by a 9D vector (XYZ, RGB, normalized spatial coordinates). We follow the training, validation and testing split from [39]. We report the results of this experiment in Table 4. We obtained higher accuracy than popular point-based networks like PointNet++ [41], PCNN [2] as well as the graph based network DGCNN [56]. Note that [30] uses different pre-processing steps. Namely, the blocks were of $1.3m \times 1.3m$, where the added $0.3m$ on each dimensions is used for location context, and is not part of the objective at each block. In addition, we compare our work with a recent paper [48] which differs from our method by its approach of combining geodesic and Euclidean data, decoupling the data by utilizing parallel networks.

4.3 Ablation study

We measure the contribution of each component of our model, as well as different combinations of them, on classification with ModelNet40. Our results read that as expected, using each component on its own (e.g., mass term only) reduces accuracy. However, by combining the different terms - accuracy increases. We found that using the mass and Laplacian term is more beneficial than the mass and gradient term. This shows the representation power of the Laplacian operator which is widely used in classical computer graphics and vision [46, 4, 43]. That is in addition to spectral-based GCNs which are parameterized by polynomials of the graph Laplacian [11, 27, 42].

In addition, we experiment with different number of neighbors, with and without pooling, reading slight reduction in performance, but with less FLOPs and memory requirements. We note that the pooling operations lead to better performance since they enlarge the receptive fields of the neurons.

5 Conclusion

We presented a novel graph convolution kernel based on discretized differential operators, which together with our AMG pooling and unpooling operators form the most important components of a CNN. Our GCN network shows on par or better performance than current state-of-the-art GCNs. We also draw an analogy between standard structured CNNs and our method, and the reduced cost of ours compared to other GCNs.

Acknowledgments and Disclosure of Funding

The research reported in this paper was supported by the Israel Innovation Authority through Avatar consortium. ME is supported by Kreitman High-tech scholarship.

References

- [1] Iro Armeni, Ozan Sener, Amir R Zamir, Helen Jiang, Ioannis Brilakis, Martin Fischer, and Silvio Savarese. 3d semantic parsing of large-scale indoor spaces. In Proceedings of the IEEE Conference on Computer Vision and Pattern Recognition, pages 1534–1543, 2016.
- [2] Matan Atzmon, Haggai Maron, and Yaron Lipman. Point convolutional neural networks by extension operators. arXiv preprint arXiv:1803.10091, 2018.
- [3] Andrew Brock, Theodore Lim, James M Ritchie, and Nick Weston. Generative and discriminative voxel modeling with convolutional neural networks. arXiv preprint arXiv:1608.04236, 2016.
- [4] Michael M Bronstein and Iasonas Kokkinos. Scale-invariant heat kernel signatures for non-rigid shape recognition. In 2010 IEEE Computer Society Conference on Computer Vision and Pattern Recognition, pages 1704–1711. IEEE, 2010.
- [5] Joan Bruna, Wojciech Zaremba, Arthur Szlam, and Yann LeCun. Spectral networks and locally connected networks on graphs. arXiv preprint arXiv:1312.6203, 2013.
- [6] Angel X Chang, Thomas Funkhouser, Leonidas Guibas, Pat Hanrahan, Qixing Huang, Zimo Li, Silvio Savarese, Manolis Savva, Shuran Song, Hao Su, et al. Shapenet: An information-rich 3d model repository. arXiv preprint arXiv:1512.03012, 2015.
- [7] Bo Chang, Lili Meng, Eldad Haber, Lars Ruthotto, David Begert, and Elliot Holtham. Reversible architectures for arbitrarily deep residual neural networks. In Thirty-Second AAAI Conference on Artificial Intelligence, 2018.
- [8] Pratik Chaudhari, Adam Oberman, Stanley Osher, Stefano Soatto, and Guillaume Carlier. Deep relaxation: partial differential equations for optimizing deep neural networks. Research in the Mathematical Sciences, 5(3):30, 2018.
- [9] Liang-Chieh Chen, George Papandreou, Iasonas Kokkinos, Kevin Murphy, and Alan L Yuille. Deeplab: Semantic image segmentation with deep convolutional nets, atrous convolution, and fully connected crfs. IEEE transactions on pattern analysis and machine intelligence, 40(4):834–848, 2017.
- [10] Tian Qi Chen, Yulia Rubanova, Jesse Bettencourt, and David K Duvenaud. Neural ordinary differential equations. In Advances in Neural Information Processing Systems, pages 6571–6583, 2018.
- [11] Michaël Defferrard, Xavier Bresson, and Pierre Vandergheynst. Convolutional neural networks on graphs with fast localized spectral filtering. In Advances in neural information processing systems, pages 3844–3852, 2016.
- [12] Inderjit S Dhillon, Yuqiang Guan, and Brian Kulis. Weighted graph cuts without eigenvectors a multilevel approach. IEEE transactions on pattern analysis and machine intelligence, 29(11):1944–1957, 2007.
- [13] Francis Engelmann, Theodora Kontogianni, Alexander Hermans, and Bastian Leibe. Exploring spatial context for 3d semantic segmentation of point clouds. In Proceedings of the IEEE International Conference on Computer Vision Workshops, pages 716–724, 2017.
- [14] Jonathan Ephrath, Moshe Eliasof, Lars Ruthotto, Eldad Haber, and Eran Treister. Leanconvnets: Low-cost yet effective convolutional neural networks, 2019.

- [15] Yifan Feng, Haoxuan You, Zizhao Zhang, Rongrong Ji, and Yue Gao. Hypergraph neural networks. In Proceedings of the AAAI Conference on Artificial Intelligence, volume 33, pages 3558–3565, 2019.
- [16] Yifan Feng, Zizhao Zhang, Xibin Zhao, Rongrong Ji, and Yue Gao. Gvcnn: Group-view convolutional neural networks for 3d shape recognition. In Proceedings of the IEEE Conference on Computer Vision and Pattern Recognition, pages 264–272, 2018.
- [17] Matthias Fey and Jan Eric Lenssen. Fast graph representation learning with pytorch geometric. arXiv preprint arXiv:1903.02428, 2019.
- [18] Hongyang Gao and Shuiwang Ji. Graph u-nets. arXiv preprint arXiv:1905.05178, 2019.
- [19] Justin Gilmer, Samuel S Schoenholz, Patrick F Riley, Oriol Vinyals, and George E Dahl. Neural message passing for quantum chemistry. In Proceedings of the 34th International Conference on Machine Learning-Volume 70, pages 1263–1272. JMLR. org, 2017.
- [20] Eldad Haber and Lars Ruthotto. Stable architectures for deep neural networks. Inverse Problems, 34(1), 2017.
- [21] Rana Hanocka, Amir Hertz, Noa Fish, Raja Giryes, Shachar Fleishman, and Daniel Cohen-Or. Meshcnn: a network with an edge. ACM Transactions on Graphics (TOG), 38(4):90, 2019.
- [22] Kaiming He, Xiangyu Zhang, Shaoqing Ren, and Jian Sun. Deep residual learning for image recognition. In Proceedings of the IEEE Conference on Computer Vision and Pattern Recognition, pages 770–778, 2016.
- [23] Kaiming He, Xiangyu Zhang, Shaoqing Ren, and Jian Sun. Identity mappings in deep residual networks. In European Conference on Computer Vision, pages 630–645. Springer, 2016.
- [24] Hiroharu Kato, Yoshitaka Ushiku, and Tatsuya Harada. Neural 3d mesh renderer. In Proceedings of the IEEE Conference on Computer Vision and Pattern Recognition, pages 3907–3916, 2018.
- [25] Tsung-Wei Ke, Michael Maire, and Stella X Yu. Multigrid neural architectures. In Proceedings of the IEEE Conference on Computer Vision and Pattern Recognition, pages 6665–6673, 2017.
- [26] Diederik P Kingma and Jimmy Ba. Adam: A method for stochastic optimization. arXiv preprint arXiv:1412.6980, 2014.
- [27] Thomas N Kipf and Max Welling. Semi-supervised classification with graph convolutional networks. arXiv preprint arXiv:1609.02907, 2016.
- [28] Roman Klokov and Victor Lempitsky. Escape from cells: Deep kd-networks for the recognition of 3d point cloud models. In Proceedings of the IEEE International Conference on Computer Vision, pages 863–872, 2017.
- [29] A. Krizhevsky, I. Sutskever, and G. Hinton. Imagenet classification with deep convolutional neural networks. Adv Neural Inf Process Syst, 61:1097–1105, 2012.
- [30] Yangyan Li, Rui Bu, Mingchao Sun, Wei Wu, Xinhan Di, and Baoquan Chen. Pointcnn: Convolution on x-transformed points. In Advances in neural information processing systems, pages 820–830, 2018.
- [31] Tsung-Yi Lin, Priya Goyal, Ross Girshick, Kaiming He, and Piotr Dollár. Focal loss for dense object detection. In Proceedings of the IEEE international conference on computer vision, pages 2980–2988, 2017.
- [32] Oren E Livne and Achi Brandt. Lean algebraic multigrid (lamg): Fast graph laplacian linear solver. SIAM Journal on Scientific Computing, 34(4):B499–B522, 2012.
- [33] Yiping Lu, Aoxiao Zhong, Quanzheng Li, and Bin Dong. Beyond finite layer neural networks: Bridging deep architectures and numerical differential equations. In International Conference on Machine Learning (ICML), 2018.
- [34] Ilay Luz, Meirav Galun, Haggai Maron, Ronen Basri, and Irad Yavneh. Learning algebraic multigrid using graph neural networks, 2020.
- [35] Jonathan Masci, Davide Boscaini, Michael Bronstein, and Pierre Vandergheynst. Geodesic convolutional neural networks on riemannian manifolds. In Proceedings of the IEEE international conference on computer vision workshops, pages 37–45, 2015.

- [36] Daniel Maturana and Sebastian Scherer. Voxnet: A 3d convolutional neural network for real-time object recognition. In 2015 IEEE/RSJ International Conference on Intelligent Robots and Systems (IROS), pages 922–928. IEEE, 2015.
- [37] Federico Monti, Davide Boscaini, Jonathan Masci, Emanuele Rodola, Jan Svoboda, and Michael M Bronstein. Geometric deep learning on graphs and manifolds using mixture model cnns. In Proceedings of the IEEE Conference on Computer Vision and Pattern Recognition, pages 5115–5124, 2017.
- [38] Adam Paszke, Sam Gross, Francisco Massa, Adam Lerer, James Bradbury, Gregory Chanan, Trevor Killeen, Zeming Lin, Natalia Gimelshein, Luca Antiga, Alban Desmaison, Andreas Kopf, Edward Yang, Zachary DeVito, Martin Raison, Alykhan Tejani, Sasank Chilamkurthy, Benoit Steiner, Lu Fang, Junjie Bai, and Soumith Chintala. Pytorch: An imperative style, high-performance deep learning library. In H. Wallach, H. Larochelle, A. Beygelzimer, F. d’Alché-Buc, E. Fox, and R. Garnett, editors, Advances in Neural Information Processing Systems 32, pages 8024–8035. Curran Associates, Inc., 2019.
- [39] Charles R Qi, Hao Su, Kaichun Mo, and Leonidas J Guibas. Pointnet: Deep learning on point sets for 3d classification and segmentation. In Proceedings of the IEEE Conference on Computer Vision and Pattern Recognition, pages 652–660, 2017.
- [40] Charles R Qi, Hao Su, Matthias Nießner, Angela Dai, Mengyuan Yan, and Leonidas J Guibas. Volumetric and multi-view cnns for object classification on 3d data. In Proceedings of the IEEE conference on computer vision and pattern recognition, pages 5648–5656, 2016.
- [41] Charles Ruizhongtai Qi, Li Yi, Hao Su, and Leonidas J Guibas. Pointnet++: Deep hierarchical feature learning on point sets in a metric space. In Advances in Neural Information Processing Systems, pages 5099–5108, 2017.
- [42] Anurag Ranjan, Timo Bolkart, Soubhik Sanyal, and Michael J Black. Generating 3d faces using convolutional mesh autoencoders. In Proceedings of the European Conference on Computer Vision (ECCV), pages 704–720, 2018.
- [43] Dan Raviv, Michael M Bronstein, Alexander M Bronstein, and Ron Kimmel. Volumetric heat kernel signatures. In Proceedings of the ACM workshop on 3D object retrieval, pages 39–44, 2010.
- [44] Olaf Ronneberger, Philipp Fischer, and Thomas Brox. U-net: Convolutional networks for biomedical image segmentation. In International Conference on Medical image computing and computer-assisted intervention, pages 234–241. Springer, 2015.
- [45] John W Ruge and Klaus Stüben. Algebraic multigrid. In Multigrid methods, pages 73–130. SIAM, 1987.
- [46] Raif M Rustamov. Laplace-beltrami eigenfunctions for deformation invariant shape representation. In Proceedings of the fifth Eurographics symposium on Geometry processing, pages 225–233. Eurographics Association, 2007.
- [47] Lars Ruthotto and Eldad Haber. Deep neural networks motivated by partial differential equations. Journal of Mathematical Imaging and Vision, pages 1–13, 2019.
- [48] Jonas Schult*, Francis Engelmann*, Theodora Kontogianni, and Bastian Leibe. DualConvMesh-Net: Joint Geodesic and Euclidean Convolutions on 3D Meshes. In IEEE Conference on Computer Vision and Pattern Recognition (CVPR), 2020.
- [49] Yiru Shen, Chen Feng, Yaoqing Yang, and Dong Tian. Neighbors do help: Deeply exploiting local structures of point clouds. arXiv preprint arXiv:1712.06760, 1(2), 2017.
- [50] Yiru Shen, Chen Feng, Yaoqing Yang, and Dong Tian. Mining point cloud local structures by kernel correlation and graph pooling. In Proceedings of the IEEE conference on computer vision and pattern recognition, pages 4548–4557, 2018.
- [51] Martin Simonovsky and Nikos Komodakis. Dynamic edge-conditioned filters in convolutional neural networks on graphs. In Proceedings of the IEEE conference on computer vision and pattern recognition, pages 3693–3702, 2017.
- [52] Karen Simonyan and Andrew Zisserman. Very deep convolutional networks for large-scale image recognition. arXiv preprint arXiv:1409.1556, 2014.
- [53] Hang Su, Subhransu Maji, Evangelos Kalogerakis, and Erik Learned-Miller. Multi-view convolutional neural networks for 3d shape recognition. In Proceedings of the IEEE international conference on computer vision, pages 945–953, 2015.

- [54] Eran Treister and Irad Yavneh. Non-galerkin multigrid based on sparsified smoothed aggregation. SIAM Journal on Scientific Computing, 37(1):A30–A54, 2015.
- [55] SY Wang, Kian Meng Lim, Boo Cheong Khoo, and Michael Yu Wang. An extended level set method for shape and topology optimization. Journal of Computational Physics, 221(1):395–421, 2007.
- [56] Yue Wang, Yongbin Sun, Ziwei Liu, Sanjay E Sarma, Michael M Bronstein, and Justin M Solomon. Dynamic graph cnn for learning on point clouds. arXiv preprint arXiv:1801.07829, 2018.
- [57] E Weinan. A Proposal on Machine Learning via Dynamical Systems. Communications in Mathematics and Statistics, 5(1):1–11, March 2017.
- [58] Zhirong Wu, Shuran Song, Aditya Khosla, Fisher Yu, Linguang Zhang, Xiaoou Tang, and Jianxiong Xiao. 3d shapenets: A deep representation for volumetric shapes. In Proceedings of the IEEE conference on computer vision and pattern recognition, pages 1912–1920, 2015.
- [59] Li Yi, Vladimir G Kim, Duygu Ceylan, I-Chao Shen, Mengyan Yan, Hao Su, Cewu Lu, Qixing Huang, Alla Sheffer, and Leonidas Guibas. A scalable active framework for region annotation in 3d shape collections. ACM Transactions on Graphics (TOG), 35(6):1–12, 2016.
- [60] Zhitao Ying, Jiaxuan You, Christopher Morris, Xiang Ren, Will Hamilton, and Jure Leskovec. Hierarchical graph representation learning with differentiable pooling. In Advances in Neural Information Processing Systems, pages 4800–4810, 2018.
- [61] Kuangen Zhang, Ming Hao, Jing Wang, Clarence W de Silva, and Chenglong Fu. Linked dynamic graph cnn: Learning on point cloud via linking hierarchical features. arXiv preprint arXiv:1904.10014, 2019.